Excitonic Effects in 11-VI Serniconductor Heterostructures [*]

V. A. Chitta[†]

Laboratoire de Spectrométrie Physique, Université Joseph Fourier, Grenoble I

BP 87, 38402 - Saint Martin d'Hères, France

The potential interest in epitaxial grown heterostructures, based on wide band gap 11-VI semiconductors, for device applications has been recognized in the last few years. Heterostructures of this type are known to have band gaps which are compatible with emission in the visible range and to exhibit non-linear optical effects. These optical properties are currently being investigated in applications such as light emitting devices, optical wave guides and optical switches. It became evident that excitonic effects play a very important role concerning the optical properties of these heterostructures, and tremendous efforts have been made to find out and describe these exciton states. In this paper we focus our attention in the excitonic effects of two different II-VI heterostructures: strained $CdTe/Cd_{1-x}Zn_xTe$ superlattices and semimagnetic $CdTe/Cd_{1-x}Mn_xTe$ multiple quantum wells.

I. Introduction

Advances in tlie growth techniques like the Molecular Beam Epitaxy (MBE) has led to high quality heterostructures consisting of alternative layers of semiconductors with different band-gap energies. The most prominent material system for these structures is based on the $GaAs/Ga_{1-x}Al_xAs$ pair. For sufficiently thin layers, this leads to the well known quantum well and superlattice structures which offer the possibility of tailoring their optical and electronic properties by an appropriate choice of the layer thickness. A rather new and much less investigated material system, for these structures, is based on the II-VI compounds, and more particularly cn the Strained-Layer Superlattices (SLS) such as $CdTe/Cd_{1-x}Zn_xTe$[1] and on Diluted Magnetic Semiconductors (DMS) such as $CdTe/Cd_{1-x}Mn_xTe$[2].

In this paper me review some interesting features of these systems obtained by optical spectroscopy. We will first discuss the combined effects of band-gap offsets and lattice-parameter mismatch on the band structure of tlie $CdTe/Cd_{1-x}Zn_xTe$ SLS. From this discussion, Exciton Binding Energies (EBE) and Exciton Oscilla-

tor Strengths (EOS) are estimated and found to vary appreciably with thr superlattice period. In the second part we will show the cffect. of a magnetic field, applied both parallel and perpendicular to the growth direction, on the optical properties of a $CdTe/Cd_{1-x}Mn_xTe$ Multiple Quantum Wells (MQW). The possibility to have a transition from type I to type 11 band structure, as well as the observed anisotropy of the Zeeman effect, are discussed.

II. $CdTe/Cd_{1-x}Zn_xTe$ superlattices

Due to the lattice-parameter mismatch, the different layers of the $CdTe/Cd_{1-x}Zn_xTe$ system are strained. Provided that the layer thicknesses are less than some strain-dependent critical values, the mismatch is accomodated by elastic strain. Resides that, this system is characterized hy a very small Valence-Band Offset (VBO), in absence of strain[3]. Therefore, the valence band configuration is essentially tailored by the internal strain imposed by the substrate of the buffer layer. Because of this strain, these superlattices will be an unusual mixed type system[4]: type I for heavy-hole excitons (electrons and heavy-holes being confined in the same material: CdTe) and type II for light-hole excitons

(electrons and light-holes being confined in CdTe and $Cd_{1-x}Zn_xTe$ respectively, giving rise to an "indirect" light-hole exciton in the real space).

A. Strain effects

Since tlie VBO, in tlie absence of strain, is almost zero[3], the band structure configuration of tlie $CdTe/Cd_{1-x}Zn_xTe$ system results from the strain, which is determined by the clioicc of tlie buffer layer. Tlie energy shift of tlie conduction band ΔV_c, and the shifts and splitting of the valence band extrema (ΔV_{hh} for heavy-holes and ΔV_{lh} foi light-holes), can be written as[5]:

$$\Delta V_c = \Delta H_c \ ,$$

$$\Delta V_{hh} = \Delta H_v + \Delta S \ , \qquad (1)$$

$$\Delta V_{lh} = \Delta H_v - \Delta S \ ,$$

with

$$\Delta H_i = 2A_i(S_{11} + 2S_{12})X \ ,$$

and

$$\Delta S = B(S_{11} - S_{12})X \ ,$$

where $(i = c, v)$, A, and A_v are the hydrostatic deformation potentials of conduction and valence band respectively, B is tlic shear deformation potential, S_{11} and S_{12} are the elastic compliance constants, and X is the in-plane stress experienced by the layers,

$$X = \frac{(a_s - a_l)}{a_l}\frac{1}{(S_{11} + S_{12})} \ , \qquad (2)$$

where a_s (a_l) is the lattice parameter of the substrate of buffer layer (layer). Foi the samples studied here, $CdTe/Cd_{1-x}Zn_xTe$ $(x = 8\%)$ we can distinguish three distinct situations, illustrated in lig. 1. With a. CdTe buffer layer (Fig. la.) the quantum well is not strained $(X_W = 0)$, since it has tlic same lattice parameter as tlie buffer layer, whereas tlic harricrs are in biaxial dilatation $(X_B > 0)$. Tlie ground state of tlie systern is tlie indirect light-hole exciton $(e_1 l_1)$. When a $Cd_{1-y}Zn_yTe$
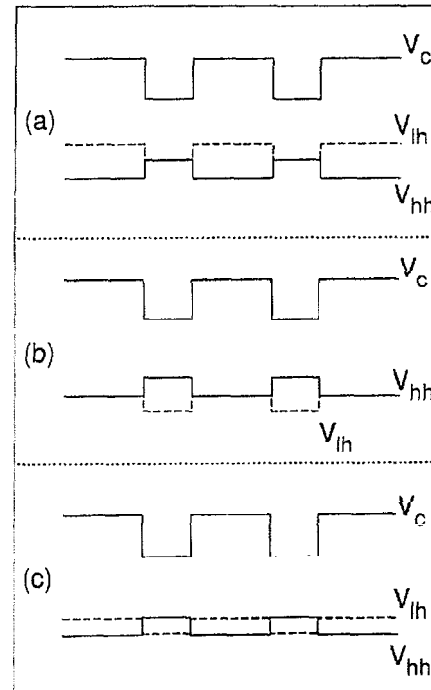

Figure 1: Schematic diagram of tlie conduction (V_c) and valence $(V_{hh}$ and $V_{lh})$ bands of a strained $CdTe/Cd_{1-x}Zn_xTe$ superlattice as a function of tlie zinc content of the $Cd_{1-y}Zn_yTe$ buffer layer. (a) y = 0; (b) y = 0.08; and (c) y = 0.04.

$(y = 8\%)$ buffer layer is used (Fig.1b), the barrier is not strained $(X_B = 0)$, but the quantum well is in biaxial compression $(X_W < 0)$. The heavy-holes are pushed above the light-holes in tlie CdTe layer, and the heavy-hole cxciton $(e_1 h_1)$ is the ground state of the system. An intermediate situation occurs when the zinc content of tlie buffer layer is in between 0% and 8%, for example y = 4% (Fig.1c). The CdTe layer is in biaxial compression and the $Cd_{1-x}Zn_xTe$ $(x = 8\%)$ layers are in biaxial dilatation. While in the well tlie heavy-holes are pushed above the light-holes, the inverse occurs in the barriers. Nevertheless, in all cases, we have a type I superlattice for the heavy-hole excitons and a type II superlattice for the light-hole ones.

B. Experiments

The samples were grown by MBE on {001}-oriented $Cd_{1-y}Zn_yTe$ (y ≈ 4%) substratcs. Most of tlie samples discussed here consist of equal thicliness layers of CdTe and $Cd_{1-x}Zn_xTe$ (with tlie amount of zinc ranging between 6% and 12%) They were grown either directly

Table I. Sample parameters. $y\%$ and $x\%$ are the zinc content of the substrate and barriers respectively, L_W and L_B the quantum well antl barrier widths, and N the number of periods.

Sample	$y\%$	$x\%$	L_W (nm)	L_B (nm)	N
S1	0.0	6.0	6.2	6.1	10
S2	0.0	8.0	6.5	6.4	10
S3	4.5	9.3	6.1	6.0	70
S4	8.4	8.4	6.5	6.4	10
S5	4.5	10.3	7.1	7.3	67
S6	3.4	8.7	3.2	3.5	67
S7	4.5	8.6	14.0	13.8	278
S8	4.4	9.9	12.8	12.6	254
S9	4.6	8.3	7.1	13.8	15
S10	5.8	10.7	13.0	20.5	30
S11	4.0	11.0	12.7	13.0	40
S12	5.0	10.8	16.9	25.3	20
S13	3.8	8.0	18.0	18.0	10

on the substrate or on a buffer layer. The structural parameters of these samples are summarized in Table I. The optical stiicly of these samples includes transmission, reflectivity, photoluminescence (PL), and photoluminescence excitation (PLE) spectra. The high quality of the structures is shown by the small linewidth and the very small Stokes shift. Transitions related to the light-hole exciton were distinguished from heavy-hole ones by polarized photoluminescence excitation (PPLE)[6].

C. Buffer layer effect

The experimental positioiis of the heavy- antl light-hole exciton transitions are plotted in Fig. 2 for tlie samples S1, S2, S3, and S4. These data are compared with the calculated direct gap E_1H_1 and indirect gap E_1L_1, plotted versus tlie average strain $\varepsilon_{\parallel}$ in tlie SLS, i.e. as a function of the Zn composition in the buffer layer that iniposes the in-plane lattice parameter.

We emphasize that the zinc concentration and the width of the barrier and tlic well layers are nearly the same for the four samples. Therefore, the depth and width of the confinement potential V_{hh} for heavy-holes and V_{lh} for light-holes are practically unchanged when one varies the buffer layer. The differences in the elastic constants and deforination poteritials between CdTe
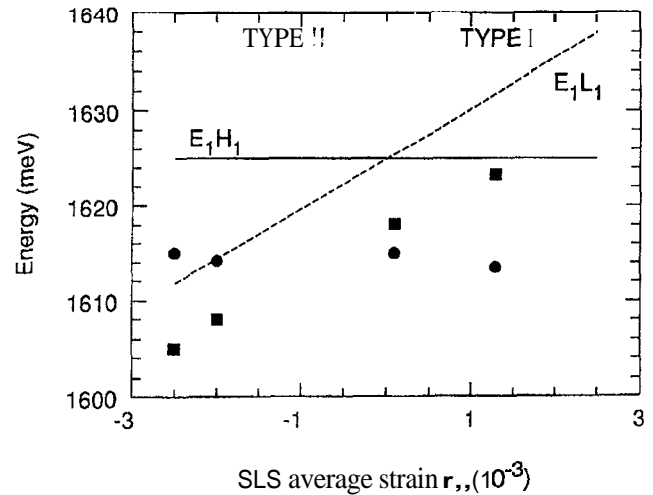

Figure 2: Influence of $\varepsilon_{\parallel}$, tlie superlattice's average in-plane strain, on the calculated gaps E_1H_1 (solid line) and E_1L_1 (dashed line) for samples with a period (6.5 nm)/(6.5 nm) and oii tlie experimeiital excitonic energies $E(e_1h_1)$ (closed circles) and $E(e_1l_1)$ (closecl squares) for samples S1, S2, **S3**, and S4. The strain $\varepsilon_{\parallel} = (a_{\text{free-standing}} - a_{\text{buffer}})/a_{\text{buffer}}$, where $a_{\text{free-standing}}$ is the in-plane lattice parameter of the hypothetical free-standing superlattice and a_{buffer} is tlie buffer's lattice parameter.

antl $Cd_{1-x}Zn_xTe$ ($x \approx 8\%$) are such that V_{hh} and V_{lh} are coiistant within an acciiracy of 1%. Varying the buffer only shifts the lieavy- and light-hole potentials as a whole relative to each other. Then, the inversion of tlie optical type in tliese superlattices is entirely due to the strain changes.

D. Influence of the period

1. binding energy and band offset

We have plotted in Fig. **3** the experimental energy positions of the e_1h_1 and e_1l_1 excitonic transitions *as* a function of tlie period of the superlattice. The solid and dashed lines represent the variations of tlie optical gaps E_1H_1 and E_1L_1 respectively, obtained using a Kronig-Penney calculation assuming that the VBO is zero in the absence of strain. The heavy-hole exciton energy $E(e_1h_1)$ follows the optical gap E_1H_1 as the period increases, which shows that, over this range of thickness, the heavy-hole EBE (of the order of 14 meV, i.e. only 40% larger than in the bulk CdTe) remains roughly constant. The experimental values of tlie light-hole EBE (i.e. the energy difference between
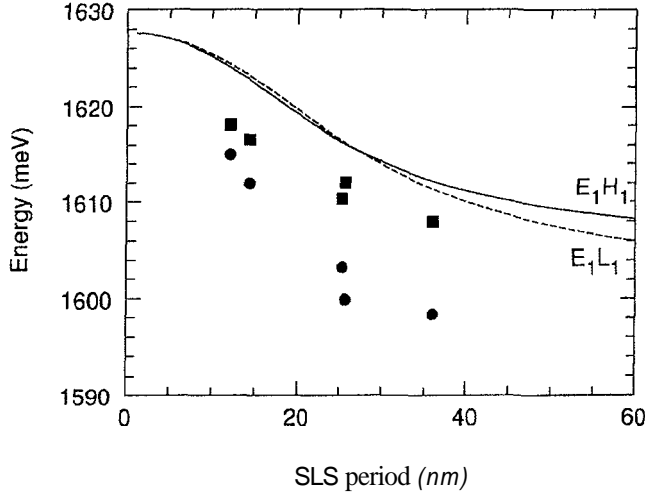
Figure 3: Calculated gaps E_1H_1 (solid line) and E_1L_1 (dashed line) versus the superlattice period for CdTe/Cd$_{1-x}$Zn$_x$Te SLS ($x \approx 0.08$, $L_{CdTe} = L_{Cd_{1-x}Zn_xTe}$; grown on a Cd$_{1-y}Zn_y$Te ($y \approx 0.04$) substrate). The closed circles and squares are the experimental excitonic energies $E(e_1h_1)$ and $E(e_1l_1)$ measured for samples S3, S5, S8, S11, and S13.

the experimental excitonic energies and the calculated optical gaps, see Fig. 3) are always smaller than the heavy-hole exciton values, which appears reasonable for an indirect exciton. Moreover, the energy position of e_1l_1 tends towards the calculated optical gap E_1L_1 as the period increases. This result is fully consistent with the indirect nature of the light-hole exciton; the larger the period, the smaller the overlap integral, and therefore, the smaller the indirect EBE.

The VBO for the heavy- and light-holes have three components. The first is due to the shear strain, which is approximately equal and opposite in the well and in the barriers, in all the samples considered here. The second component is the so-called chemical offset AV, which is often expressed as a fraction δ of the energy gap difference ΔE_g between the well and barrier. The third component is a hydrostatic strain term which depends on the absolute deformation potential A, of the valence bands of the two materials. These absolute deformation potentials are not accessible by piezospectroscopic experiments, which measures the relative deformation potential, A = A, $- A_v$, of the conduction- and valence-band edges in the same material. The second and third components cannot be determined independently, so we will call the sum of these two components the "aver-

age band offset" AV, the average being over the light- and heavy-hole band edges. Note that the conduction-band offset is determined by AV, since ΔE_g and A are known. To estimate AV, we will analyse the binding energy of the light-hole exciton.

The observed 1S exciton energy for the spatially direct (heavy-hole) and indirect (light-hole) transitions may be expressed as:

$$E(e_1h_1) = E_g^W + \Delta H_c^W + \Delta H_v^W - \Delta S^W$$
$$+ E(E_1) + E(H_1) - E_{hh} , \qquad (3)$$

and

$$E(e_1l_1) = E_g^W + \Delta H_c^W + \Delta H_v^W - \Delta V_a - \Delta S^B$$
$$+ E(E_1) + E(L_1) - E_{lh} . \qquad (4)$$

Here $E_g^W = 1.606\,\mathrm{eV}$ is the band gap of the bulk CdTe, $\Delta H_c^W + \Delta H_v^W$ the hydrostatic strain shift of the conduction band edge in the CdTe layer relative to the valence band, AV, the average VBO, AS^W the shear strain shift of the heavy-hole band in the CdTe layer, and ΔS^B that of the light-hole band in the Cd$_{1-x}$Zn$_x$Te layer. $E(E_1)$, $E(H_1)$, and $E(L_1)$ are, respectively, the electron, heavy-hole, and light-hole confinement energies in the n = 1 subband, and E_{hh} and E_{lh} are the respective EBE's. In principle all of these parameters are accurately known, the only unknown one is AV, which is taken as an adjustable parameter.

Since the heavy-hole transition energy does not depend explicitly on AV, we will concentrate our analysis on the light-hole transition energy. Fig. 4 shows the light-hole EBE as a function of the superlattice period. The points are the experimentally determined EBE obtained from the difference between the optical gap E_1L_1, calculated using different values of **A**V_a, and the measured transition energies $E(e_1l_1)$. The two lines are calculated binding energies using the method of Leavitt and Little[7]. The lowest curve is obtained for a light-hole in-plane effective mass given by $(\gamma_1 - \gamma_2)^{-1}$ where γ_1 and γ_2 are the Luttinger parameters. The highest curve, which is calculated using an infinite in-plane effective mass, represents an upper limit. The
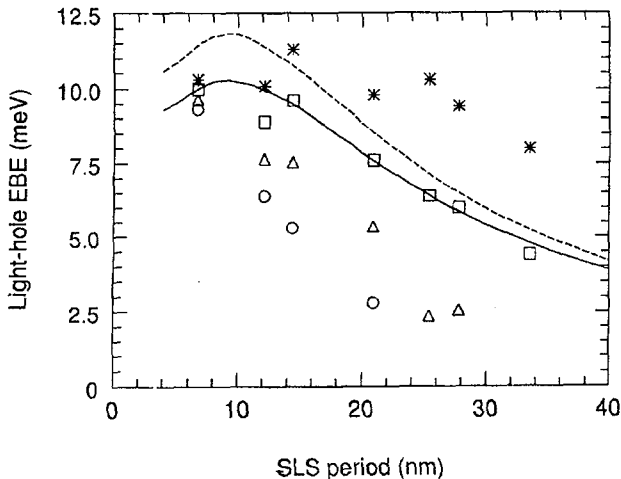
Figure 4: Experimentally determined light-hole exciton binding energy, of samples S3, S5, S6, S7, S8, S9, and S10, for different values of ΔV_a: $-0.08\Delta E_g$ (stars), $+0.02\Delta E_g$ (squares), $+0.13\Delta E_g$ (triangles), and $+0.22\Delta E_g$ (circles). The lines are the calculated light-hole exciton binding energy using an in-plane effective mass given by the Luttinger parameters $(\gamma_1 - \gamma_2)^{-1}$ (solid line) and an infinite mass (dashed line).

best agreement between theory and experimental results is obtained for a $\Delta V_a = 0.02$ (± 0.04) ΔE_g. Thus, it appears that within our experimental accuracy the average VBO in this system is indeed zero.

2. oscillator strength

The oscillator strength is an useful quantity to characterize the strength of an optical transition, which can help in the identification of direct and indirect excitons. The EOS per quantum well is defined by[8]:

$$f_{2D} = f_{3D}\,\pi\,(a^*_{\varepsilon D})^3 \left(\frac{\mu_{2D}}{\mu_{3D}}\right)^2 \left|\int c(z)v(z)dz\right|^2 |\varphi(\rho = 0)|^2 , \tag{5}$$

where a^*_{3D} is the 3D exciton Bohr radius (≈ 7 nm for CdTe), $c(z)$ and $v(z)$ are the envelope functions describing the electron and hole motion along the growth axis, $\varphi(\rho)$ describes the in-plane relative electron-hole motion and μ is the electric dipole matrix element between the conduction and valence bands Bloch states: $(\mu_{2D}/\mu_{3D})^2 = 3/4$ and $1/4$ for heavy- and light-hole respectively. f_{3D} is the 3D EOS which is given by:

$$f_{3D} = \frac{m_0}{\hbar^2} \frac{\epsilon_\infty}{\alpha \lambda_0} \Delta E_{LT}, \tag{6}$$

with ϵ_∞ the high-frequency dielectric constant (for CdTe $\epsilon_\infty = 7.4$), α the constant of fine structure ($\alpha = 1/137$), and λ_0 the wavelength of the excitonic transition ($\lambda_0 \approx 770$ nm for the structures studied). ΔE_{LT} is the longitudinal-transverse splitting of the excitonic polariton, $\Delta E_{LT} \approx 0.9$ meV, as determined from reflectivity measurements[9]. Using these values we obtain for CdTe $f_{3D} \simeq 1.6 \times 10^{-2}$ nm^{-3}.

The measured EOS is obtained from the integrated absorption spectra[8] assuming that in a MQW structure the absorption of each quantum well adds linearly, which gives:

$$\int_{line} \Lambda(E)dE = \frac{2\pi\hbar^2}{m_0 n}\alpha N f_{2D} , \tag{7}$$

where $\Lambda(E)$ is the absorption coefficient as a function of the energy, N is the number of quantum wells, and n is the refractive index.

The experimental results for the heavy-hole EOS (closed circles in Fig. 5) show a great dispersion which can be due to the difficulty of measuring large optical densities and/or to the assumption that the quantum well absorption adds linearly independently of the barrier thickness. Nevertheless the average value measured for the $e_1 h_1$ EOS coincides with the theoretical estimation made using the bulk ΔE_{LT}. For the light-hole the theory predicts an important reduction of the oscillator strength at large superlattice periods due to the spatial separation of electrons and holes and the resulting decrease of the wavefunction overlap. Experimentally the $e_1 l_1$ EOS (closed squares in Fig. 5) is found to be essentially independent of the superlattice period which strongly desagrees with the theoretical prediction. This points toward a highly correlated motion of the electron-hole pair which leads to the formation of an interface exciton. This localisation could be enhanced by a surface electric field or by structural differences between the two interfaces.

III. Cdte/Cd$_{1-x}$Mn$_x$ multiple quantum wells

In the CdTe/Cd$_{1-x}$Mn$_x$Te system the replacement of the Cd atoms by those of the Mn alters not only the band-gap energy[10], but also leads to an exchange
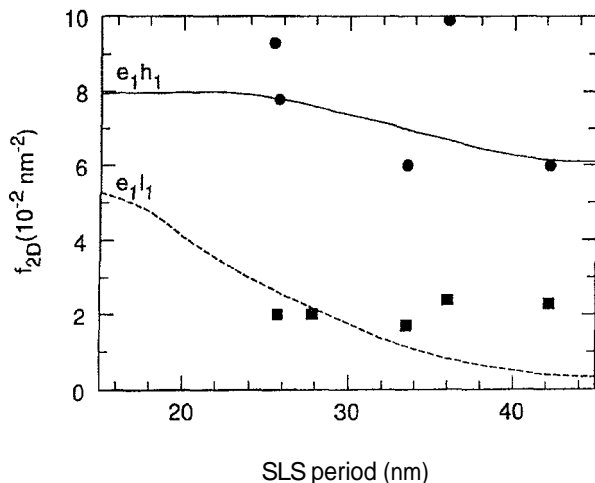
Figure 5: Oscillator strength measured for $e_1 h_1$ (closed circles) ancl $e_1 l_1$ (close squares) for samples S7, S8, S10, S11, S12, and S13. The lines show tlie results obtained for $e_1 h_1$ (solid line) and $e_1 l_1$ (dashed line) using eq. (5).

interaction between tlie spins of the carriers essentially confined in tlie CdTe layers, and those of the paramagnetic Mn^{2+} ions located in the $Cd_{1-x}Mn_x Te$ barriers[11]. These exchange effects cause a. lot of nem spin dependent phenomena like large Faraday rotation[12], magnetic polarons[13,14], and their dynamical behavior[15,16]. Noticeably, the formation of the magnetic polarons is expected to greatly influence tlie recombination dynamics in these structures. However, tlie far most spectacular property, due to the spin excliange, is the so-called giant Zeeman splitting of the band edges[17]. Thus, the application of an external magnetic field at low temperature opens the unique possibility of a magnetic tuning of the barriers heights experienced by the carriers[18,19].

A. Experimental details

The structures investigated were pseudomorphically grown by MBE on a {001}-oriented InSb substrate. The growtli temperature was 235°C. Further details of tlie growth are given in reference [20]. The growth was initiated by a 0.1μm layer of CdTe ancl the MQW stack clad between two 0.15μm layers of $Cd_{1-x}Mn_x Te$, ench with tlie same manganese content as the barrier layers. The two samples described in cletail here were each grown with eight wells of widths 7.5 and 35 nm respectively. We refer to these as samples I and II (see Table

Table II. Structural parameters and observed exciton transition energies for samples I and II. All energies are given in meV, ancl tlie well (L_W) and barrier (L_B) widths in nm.

Sample	L_W	L_B	$e_1 h_1$(1S)	$e_1 h_1$(2S)	$e_1 l_1$
I	7.5	20	1619.2	1639.2	1626.2
II	15	20	1602.6	1615.2	1607.3

II). Tlie barrier thickness were 20 nni in each structure.

Magneto-optical investigations were carrier out with the samples mounted, strain free, in a superconducting magnet, and immersed in overpumped liquid helium. Photoluminescence (PL) and photoluminescence excitation (PLE) were performed in both Faraday and Voigt configurations with the sample excited by a pyridine dye laser. Since the magnetization of the samples vary strongly with temperature the sample temperature lias to be carefully controlecl; therefore to avoid heating of the manganese spin system the laser beam was loosely focused with a. power level mantained bellow 0.01 W/cm^2.

B. Zero-field spectra

PL and PLE spectra of sample II are shown in Fig. 6. The lines observed in both spectra at 1602.6 meV are due to tlie $e_1 h_1$ free exciton. The absence of a Stokes shift ancl the small linewidths, ≈ 1 meV, are representative of good quality samples. The relative intensity of tlie PL line observed 2.8 meV below the free exciton line decreases as the laser power is increased; we assign it to an exciton trapped on a donor. A polarized PL study[21] sliowed that the line at 1607.3 meV is related to a liglit-hole transition; it is assigned to the $e_1 l_1$ exciton. The large diamagnetic shift observed leads us to assign the 1615.2 meV line to the 2s state of the $e_1 h_1$ free exciton. Sample I has similar spectra.

C. Parallel magnetic field

Due to the exchange interaction between the carriers ancl tlie magnetic ions, it is possible to tune tlie band-gap of the magnetic layers, and hence the conduction- and valence-band offsets, by application of
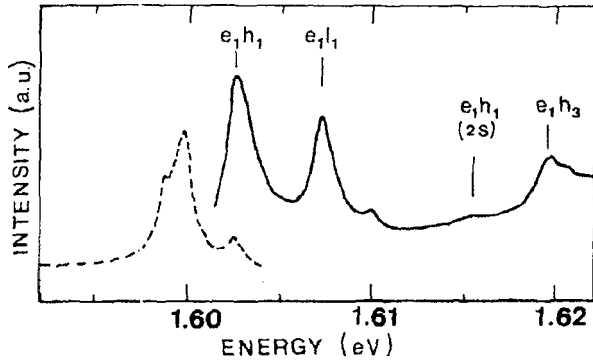
Figure 6: Photoluminescence (dashed line) and photoluminescence excitation (solid line) spectra of sample II at 1.45 K. The excitation spectrum was recorded whilst monitoring the impurity band at 1596 meV.

a magnetic field. Thus the applied field can induce large changes of the carrier confinement energies and the EBE[18,22]. Eventually if the changes of the band offset are large enough a field-induced transition of the MQW from type I (direct ground state transition in real space) to type II (indirect ground state transition in real space) may take place. Such transition have been observed by Liu et. al.[23] in ZnSe/Zn$_{1-x}$Fe$_x$Se structures and by Deleporte et. al.[24] in {111}-grown CdTe/Cd$_{1-x}$Mn$_x$Te structures with $x = 6.7\%$. However, in a (001) CdTe/Cd$_{1-x}$Mn$_x$Te structure with the same manganese concentration Wasiela et. al.[18] found no evidence for this transition. In an attempt to better understand this transition, we have chosen MQW samples with small manganese concentrations in the range of 3% to 5%, as described above. This range was chosen because at small manganese concentrations the relative variations of the band offset with magnetic field are the largest. This occurs because it is only at very small x ($< 2\%$) that the magnetic susceptibility of Cd$_{1-x}$Mn$_x$Te increases linearly with x [17]. At higher concentrations the susceptibility increases less rapidly and eventually decreases at $x > 15\%$ as more and more manganese ions form antiferromagnetically coupled pairs which do not contribute to the susceptibility. On the other hand the band-gap of Cd$_{1-x}$Mn$_x$Te, and hence the band offsets, vary linearly with x. Thus the type I to type II transition should be most readily observed at low x values. At low x values the barrier heights, and hence the carrier confinement ener-

gies, are small and may be comparable with the EBE's of about 15 meV so that the interpretation of the low-temperature optical spectra requires a precise determination of the EBE's. All additional advantage of using low-x Cd$_{1-x}$Mn$_x$Te layers is that the lattice mismatch to the InSb substrate is small, 0.07% ate $x = 5\%$, and pseudoinorphic structures of high quality can be grown.

In Fig. 7 the Zeeman splitting of the PLE lines measured at 1.5 K is shown for sample II with a magnetic field applied parallel to the growth axis. Each line splits into a doublet with the σ^+ and σ^- components nearly 100% polarized. The splittings are larger by one order of magnitude than those observed in the non-magnetic CdTe/Cd$_{1-x}$Zn$_x$Te structures. The effect of applying a magnetic field, parallel to the growth direction, to the MQW structure is shown in Fig. 8. The magnetic field causes large changes in the barrier heights which in turn result in changes of both the carrier confinement energies and the EBE's[18,22].

We now describe various simulations which show that the large band-gap decrease, expected to be observed in σ^+ polarization at the type I to type II transition, may be fully compensated by a simultaneous decrease of the EBE. We first discuss the three diagrams on the left-hand side of Fig. 9 which refer to sample II. The band-gaps are calculated in the effective mass approximation with the heavy- and light-hole longitudinal effective masses given in terms of the Luttinger parameters $(\gamma_1 \mp 2\gamma_2)^{-1}$. Because the Mn composition in the alloy is small, the Luttinger parameters are taken from the CdTe optical data[25] for both CdTe and Cd$_{1-x}$Mn$_x$Te. The binding energies have been calculated with a variational model that is applicable to quantum wells with a small or negative valence band offset[24].

In the upper diagram of Fig. 9(a) the shifts of the band-gap are very asymmetrical, due to the larger relative variation of the +3/2 VBO with magnetic field. The arrows indicate the type I to type II transition. In the centre diagram (b) we show the binding energies, E_B^+ and E_B^- of the σ^+ and σ^- heavy-hole excitons as a function of the magnetic field. Large variations of the E_B^+ are observed in the vicinity of the type I to
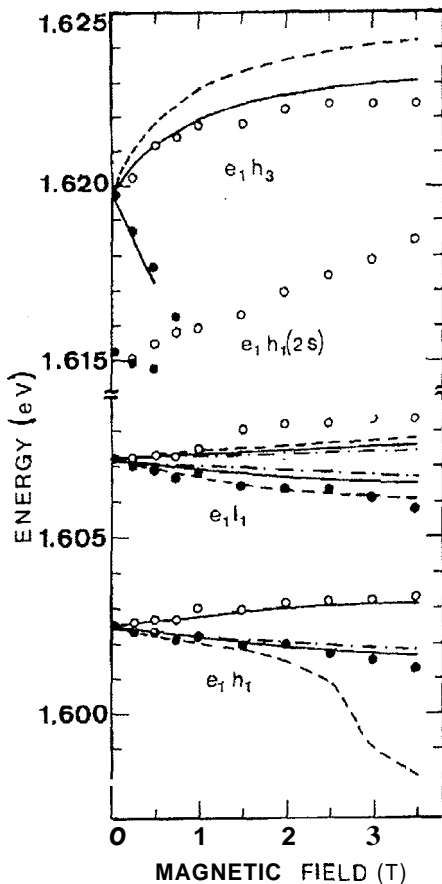
Figure 7: Zeeman spliting of tlie exciton lines observed in sample II at 1.45 K, with closed circles the σ^+ and tlie open circles tlie σ^- polarizations. Tlie curves show predicted splittings for different values of 6, tlie fraction of tlie band offset in the valence band: $\delta = 0.2$ (daslied lines), $\delta = 0.3$ (solid lines), and $6 = 0.4$ (dashed-dotted lines).
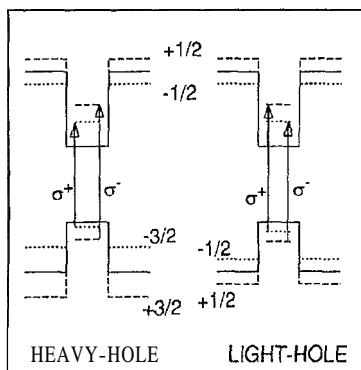

Figure 8: Effect of a inagnetic field applied parallel to tlie growth axis on the bantl edges of a $CdTe/Cd_{1-x}Mn_xTe$ quantum well. Tlie solid lines show tlie band edges at zero inagnetic field while tlie effect of applying a magnetic field is shown by the changes in tlie barriers height given by the dashed and dotted lines. The dotted and daslied lines iuside of the quantum well represent the energy of tlie confined states of the corresponding qiiantum wells formed by the dotted and daslied barriers. Tlie σ^+ and σ^- optical transitions observed in PLE are shown by the vertical arrows.

type II transitions; as the valence band barrier height approaches zero, E_R^+ approaches the three-dimensional values, 10 meV, and for higher inagnetic fields the binding energy reaches a plateau of about 5 mev for $6 = 0.2$. In the lower diagram (c) we show the energy shifts of the σ^+ and σ^- excitons, calculated from the difference of tlie two upper curves. Because the band-gap and binding energy variations counteract, the shape of the lower curve can depend niarkedly on the value of the assumed VBO and of tlie other parameters such as tlie width of the quantum well. This is well illustrated when data for $\delta = 0.2$ and 0.3 are compared.

Tlie three diagrams on the right-hand side of Fig. 9 apply to sample I and illustrate the effect of reducing the quantum well width from 15 to 7.5 nm. Whilst the magnetic-field-induced changes of the hinding energy remain nearly the same, the band-gap variations in sample I are much larger than those of sample II as a result of tlie larger confinement energies. Consequently the variations of the exciton energies with applied field are also larger. The lower diagram (c) also shows that for sample I there is no clear signature of a type I to type II transition whereas there is a clear step-like feature for sample 11 when $\delta = 0.2$.

The great sensitivity of the shape of the magnetic variation of the σ^+ e_1h_1 exciton energy to the various parameters such as band offset and quantum well width may explain the previously reported[24] observation of a plateau in a sample similar to I. However, this sample was grown along the $\{111\}$ direction so that the strain-induced piezoelectric field may also be at the origin of these differences. The experimental Zeeman data for tlie two samples are also shoivn in the lower diagrams. For sample II the date indicate a value of δ equal to 0.3 or larger. Simulations for $5 = 0.4$ are not significantly different from those of 0.3. Thus these data are consisting with the measurements previously reported[18] on a superlattice with well and barrier widths of 7.5 nm and with a manganese composition of 6.7%. The magnetic splittings observed for sample I are larger than those calculated assuming $6 = 0.3$. This may be due to a slight diffusion of manganese into the quantum well where interaction with the carrier is high. The en-
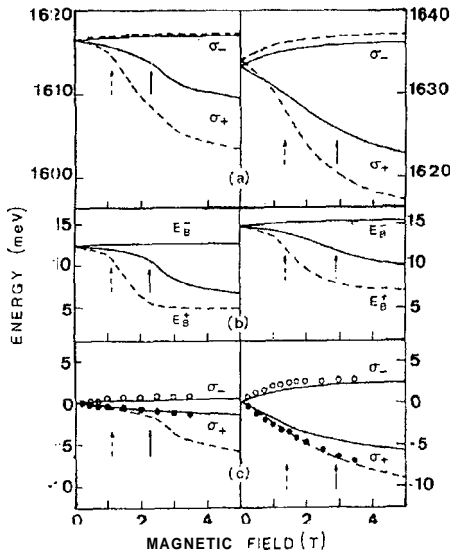
Figure 9: Calculated variation with magnetic field of (a) the band-gap energies, (b) the binding energies, and (c) the transition energies of the heavy-hole exciton for sample II (left part of the figure) and sample I (right part). The calculation are shown for two values of 6, the fraction of the total band offset in the valence band: $6 = 0.3$ (solid lines) and $6 = 0.2$ (dashed lines). The arrows indicate the magnetic field at which the type I to type II transitions occurs. The points show the experimental data.

hancement of the Zeeman effect due to such a diffusion in a smooth interface can be very large in a quantum well with a high Mn content in the barrier[18]. This effect, if not taken into account will lead to a significant underestimation of the VBO.

D. Perpendicular magnetic field

We analyse now the Zeeman splitting observed for a magnetic field applied perpendicular to the growth direction. Due to the anisotropy of the valence band, the Zeeman effect shows a complex behavior: very strongly asymmetric splittings are observed, reflecting the variation of the 'best" quantization axis from the growth direction at zero field to the magnetic-field direction. At low field the four lowest valence-band eigenstates are well described in terms of heavy- and light-holes states and the Zeeman splitting within the heavy-hole doublet is quite small as is also the case in non-magnetic heterostructures[26]. At high field the best quantization axis is along the field direction and large Zeeman shifts are observed.

The PLE spectra of sample I shown in Fig. 10 were measured in the Voigt configuration while monitoring the $D^0 X$ emission. The field was applied perpendicular to the growth direction and the laser beam was polarized either parallel (π) or perpendicular (C) to the applied field.
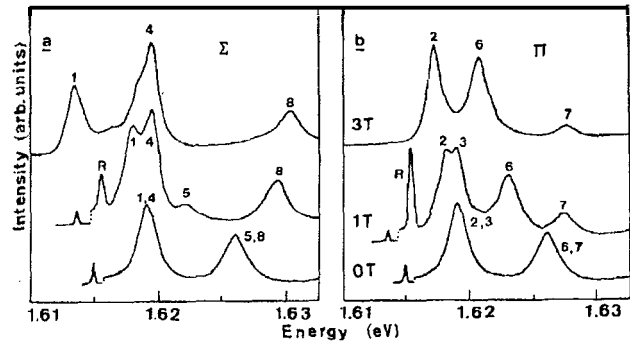

Figure 10: Photoluminescence excitation spectra measured in the Voigt configuration with the magnetic field equal to 0, 1, and 3 T. (a) C and (b) π polarizations. The lines are noted $1, 2, \ldots, 8$ in accordance with the transitions identified in Fig. 12. The R line is due to Raman scattering.
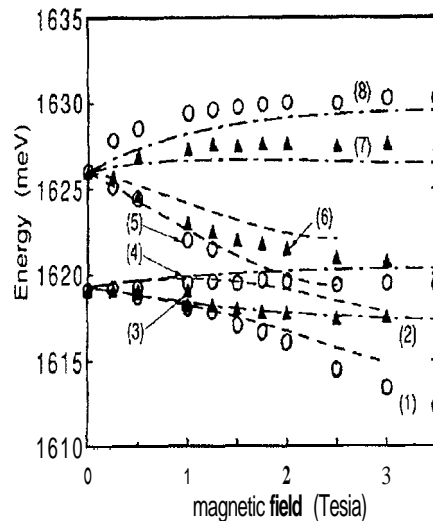

Figure 11: Zeeman splittings observed at 1.45 K (circles - C polarization; triangles - π polarization). The curves show the calculated Zeeman shifts: dashed lines show transitions originating from the $|l, 1/2\rangle$ and $|h, -3/2\rangle$ valence-band states; dashed-dotted lines show transitions originating from the $|l, 3/2\rangle$ and $|h, -1/2\rangle$ valence-band states. The numbers correspond to the lines shown in Figs. 10(a) and Figs. 10(b) and to the transitions identified in Fig. 12.

The lines observed at 1619.2 and 1626.2 meV in zero field are assigned to the $e_1 h_1$ and $e_1 l_1$ excitons respectively. In an applied field each line splits into two C and two π components. Thus, eight transitions are observed. Their energies are plotted in Fig. 11 as a function of the magnetic field. This fan diagram

is very different from the one observed when the magnetic field is applied parallel to the growth direction (Fig. 7). In Faraday configuration both the heavy- and light-hole excitons split nearly symmetrically into two components with opposite circular polarization σ^+ and $\sigma-$. In Voigt configuration, at small field, the Zeeman splitting of the heavy-hole exciton is very small, as expected theoretically and as observed[26] in non-magnetic quantum wells. At high field large splitting is observed due to large mixing of the heavy- and light-hole states induced by the magnetic field.

The Zeeman splittings have been calculated[27] for a CdTe quantum well surrounded by $Cd_{1-x}Mn_xTe$ barriers with a magnetic field applied perpendicular to the growth direction. The result of this calculation is shown in Fig. 12a. The notation of the confined eigenstates[27] $|v, m\rangle$ reflects their behavior at zero field. ($v = h$ and l refers to heavy- and light-holes) and at high field (the eigenstates are labeled $m = +3/2, +1/2, -1/2, -3/2$ in order of increasing energg). We can see in Fig. 12 that at small field the heavy-hole Zeeman splitting is vanishingly small. One also notice the anticrossing of the $|l, +1/2\rangle$ and $|h, -3/2\rangle$ states at 2 T. For comparison, the Zeeman splittings calculated for a field applied along the growth axis are shown in Fig. 12b. As already noticed, the splitting in the conduction band is independent of the orientation of the magnetic field. Opposite to that, the valence-band Zeeman effect is strikingly anisotropic.

The energies of the transitions allowed in C and π polarizations, calculated using the confinement energies shown in Fig. 12 and assuming an EBE independent of the magnetic field and equal to 13 meV are plotted iii Fig. 11. A good overall agreement between the theoretical results and the experimental data is observed. At small field, the lines involving heavy-holes exhibit much smaller splitting than those involving light-holes. The splitting between lines 8 and 7. which involve transitions originating from the same $|l, +3/2\rangle$ valence band states, measures the Zeeman effect in the conduction band. This is also true for lines 6 and 5, which involve transitions originating from the $|l, +1/2\rangle$ valence band states. Therefore, these two splitting should be equal,

which is not the case; the measured splitting originating from $|l, +3/2\rangle$ is appreciably larger than the one from $|l, +1/2\rangle$. We attribute this difference to excitonic effects. Analyzing the Zeeman effect observed for a field applied along the growth axis, we can see that the exciton binding energy varies rapidly with the magnetic field. This is specially true for samples with low manganese concentration in the barrier where the offset of the -3/2 subband may become very small or even negative (type II structures). We recently measured spin-flip resonant Raman scattering for a field applied in the plane of the layer, i.e. we directly measured the conduction-band Zeeman splitting. We found a value which is intermediate between the two values measured in the present experiment.

IV. Summary

In the first part of this paper we have shown the effect of changing the buffer layer on the band structure of a SLS CdTe/$Cd_{1-x}Zn_xTe$. We also show that the exciton binding energy of type II e_1l_1 excitons decreases at large superlattice periods as predicted theoretically. The corresponding variations of the oscillator strength are not observed experimentally. The origin of these discrepancies would deserve more elaborated calculations taking into account the valence band mixing and a possible excitons localisation near an interface.

For the CdTe/$Cd_{1-x}Mn_xTe$ MQW system with small manganese content in the barriers, we have shown that a type I to type II transition takes place at moderate magnetic field applied along the growth axis. The Zeeman energy shift of the σ^+ heavy-hole exciton does not show any clear signature, such as a step or a plateau, at the transition. Calculations show that this is due to the nearly perfect compensation of the magnetic variations of the band-gap and of the exciton binding energy. A magnetic field applied perpendicular to the growth direction induces large mixing of the valence-band subbands. This mixing occurs independently in the (-3/2, $1.2) and (+3/2, -1/2) manifolds. It reflects the variation of the best quantization axis from the growth axis toward the magnetic-field direction. A calculation of the Zeeman splittings made
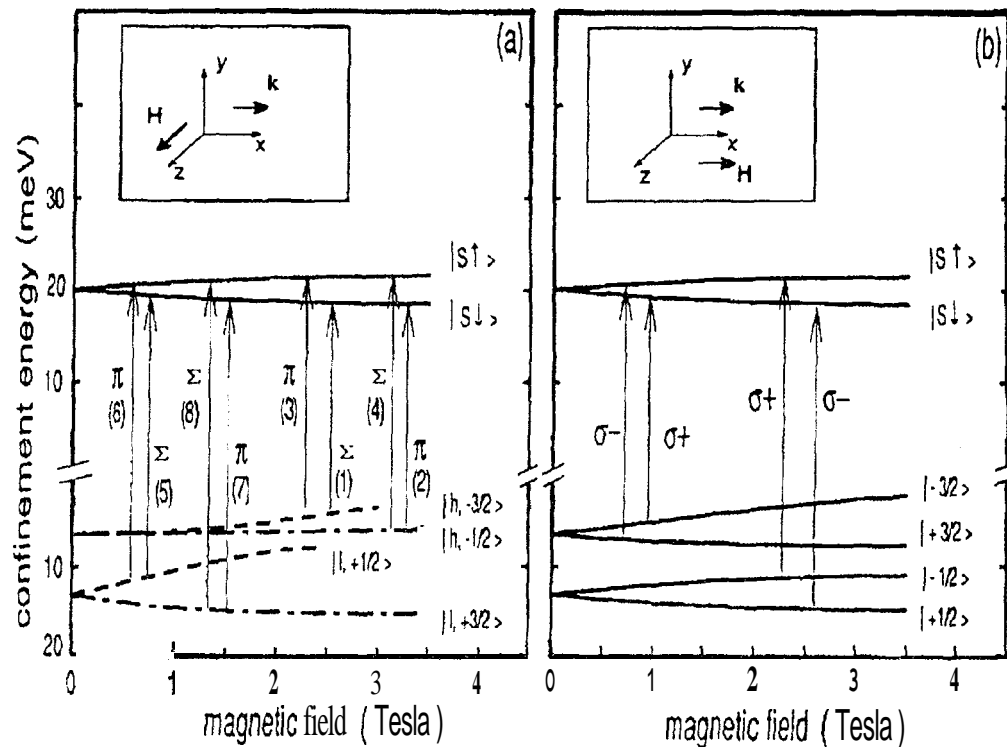
Figure 12: Quantum well energy levels as a function of the magnetic field: (a) in-plane field, allowed transitions in C and π polarizations. The numbers correspond to the lines shown on the experimental spectra of Figs. 10(a) and 10(b). (b) field applied parallel to tlie growth axis

in the envelope-function approximation accounts fairly well for the experimental results. The remaining diçcrepancies are probably due to variation of tlie exciton binding energies with the magnetic field.

Acknowledgements

References

1. H. Mariette, F. Dal'bo, N. Magnea, G. Lentz, and H. Tuffigo, Phys. Rev. B 38, 12443 (1988).

2. R. N. Bicknell, R. W. Yanka, N. C. Giles-Taylor, D. K. Blanks, E. L. Buckland, and J. F. Schetzina, Appl. Phys. Lett. 45, 92 (1984).

3. H. Mathieu, A. Chatt, J. Allegre, and J. P. Faurie, Phys. Rev. B 41, 6082 (1990).

4. J. Y. Marzin, M. N. Charasse, and B. Sermage, Pliys. Rev. B 31 8298 (1985).

5. F. H. Pollak aiid M. Cardona, Phys. Rev. 172, 816 (1968).

6. H. Tuffigo, A. Wasiela, N. Magnea, H. Mariette, and Y. Merle d'Aubigné, Phys. Rev. B 43, 14629 (1991).

7. R. P. Leavitt and J. W. Little, Phys. Rev. B 42, 11774 (1990).

8. L. C. Andreani and F. Bassani, Phys. Rev. B 41, 7536 (1990).

9. Y. Merle d'Aubigné, Le Si Dang, A. Wasiela, N. Magnea, F. Dal'bo, and A. Million, Proceedings of the 3rd Conference on Modulation Semiconductor Structures, Montpellier 1987, J. Phys. (Paris) 48, C5-363 (1987).

10. For a recent review see, e.g.: J. A. Gaj, in Semiconductors and Semimetals, Vol. 25, edited by J. K. Furdyna and J. Kossut (Academic Press, Boston, 1988) p. 275.

11. J. K. Furdyna, J. Appl. Phys. 53, 7637 (1982).

12. M. Kohl, M. R. Freeman, J. M. Hong, and D. D. Awshalom, Phys. Rev. B 43, 2431 (1991).

13. D. R. Yakovlev, W. Ossau, G. Landwehr, R. N.

Bicknell-Tassius, A. Waag, and I. N. Uraltsev, Solid State Commun. 76, 325 (1990).

14. G. E. Marques, V. A. Chitta, M. H. Degani, and H. Hipolito, Surface Sci. 196, 659 (1988).

15. D. D. Awshalom, M. R. Freeman, N. Samarth, H. Luo, ancl J. K. Furdyna, Phys. Rev. Lett. 66, 1212 (1991).

16. M. R. Freeman, D. D. Awshalom, J. M. Hong, and L. L. Chang, Phys. Rev. Lett. 64, 2430 (1990).

17. J. A. Gaj, R. Planel, and G. Fishman, Solid State Commun. 29, 435 (1979).

18. A. Wasiela, Y. Merle d'Aubigné, J. E. Nicholls, D. E. Ashenford, and B. Lunn, Solid State Coinmun. 76, 263 (1990).

19. E. Deleporte, J. -M. Berroir, G. Bastard, C. Dela-lande, J. M. Hong, and L. L. Chang, Phys. Rev. B 42, 5891 (1990).

20. G. M. Williams, A. G. Cullis, C. R. Whitehouse, D. E. Ashenford, and B. Lunn, Appl. Phys. Lett. 55, 1303 (1989).

21. Y. Merle d'Aubigné, Le Si Dang, F. Dal'bo, G. Lentz, N. Magnea, and H. Mariette, Superlatt. Microstruct. 5, 367 (1989).

22. S. K. Chang, A. V. Nurmikko, J. -W. Wu, L. A. Kolodziejski, and R. L. Gunshor, Phys. Rev. B 37, 1191 (1988).

23. X. Liu, M. Petrou, J. Warnock, B. T. Jonker, G. A. Prinz, and J. J. Krebs, Phys. Rev. Lett. 20, 2280 (1989).

24. E. Deleporte, J. -M. Berroir, G. Bastard, C. De-lalande, J. M. Hong, and L. L. Chang, Superlatt. Microstruct. 8, 171 (1990).

25. Ch. Neuman, A. Nothe, and N. O. Lipari, Phys. Rev. B 37, 922 (1988).

26. A. Fasolino, G. Platero, M. Potemski, J. C. Maan, K. Ploog, and G. Weimann, Surface Sci. 267, 509 (1992).

27. P. Peyla, A. Wasiela, Y. Merle d'Aubigné, D. E. Ashenford, and B. Lunn, Phys. Rev. B. 47, 3783 (1993).